• Clinical Research •

Multimodal imaging features of optic disc melanocytoma in a Chinese population

Yan-Ni Yan, Yue-Ming Liu, Wen-Bin Wei

Beijing Tongren Eye Center, Beijing Key Laboratory of Intraocular Tumor Diagnosis and Treatment, Beijing Ophthalmology & Visual Sciences Key Lab, Medical Artificial Intelligence Research and Verification Key Laboratory of the Ministry of Industry and Information Technology, Beijing Key Laboratory of Intelligent Diagnosis, Treatment and Prevention of Blinding Eye Diseases, Beijing Tongren Hospital, Capital Medical University, Beijing 100730, China

Correspondence to: Wen-Bin Wei. Beijing Tongren Eye Center, Beijing Tongren Hospital, No.1 Dongjiaominxiang, Beijing 100730, China. weiwenbintr@163.com

Received: 2026-02-19 Accepted: 2026-04-22

Abstract

● **AIM:** To characterize the multimodal fundus imaging features of optic disc melanocytoma (ODM) in a Chinese population.

● **METHODS:** This retrospective observational case series included patients diagnosed with ODM at Beijing Tongren Hospital between January 2015 and December 2025. Demographic data and multimodal fundus imaging findings were reviewed and analyzed.

● **RESULTS:** Sixty-nine patients (69 eyes) were included. The mean age at presentation was 47.8±12.1y (range, 17–70y), with a female predominance (71.0%). All cases were unilateral. Clinically, lesions appeared as elevated gray-to-black masses involving the optic disc. The mean basal diameter was 3.84 mm, and the mean tumor thickness was 1.68 mm. Associated findings included optic disc edema (69.6%), retinal nerve fiber layer thinning (56.5%), perivascular sheathing (33.3%), retinal edema or exudation (5.8%), epiretinal membrane (7.2%), vitreous seeding (13.0%), and peripapillary hyperreflective ovoid mass-like structures (PHOMS, 19.0%). On optical coherence tomography (OCT), the tumor-retina interface was classified into three patterns: smooth hyperreflective (27 eyes), nodular hyperreflective (34 eyes), and honeycomb-like hyperreflective (9 eyes).

● **CONCLUSION:** Chinese patients with ODM demonstrate clinical and multimodal imaging characteristics comparable to those reported in other ethnic populations. However, tumors in this cohort are slightly larger, and are associated with two relatively uncommon complications: PHOMS and epiretinal membrane. Three distinct OCT tumor-retina interface patterns were identified, which may reflect variations in tumor-retinal interaction.

● **KEYWORDS:** optic disc melanocytoma; multimodal imaging; Chinese population; peripapillary hyperreflective ovoid mass-like structures

DOI:10.18240/ijo.2026.07.15

Citation: Yan YN, Liu YM, Wei WB. Multimodal imaging features of optic disc melanocytoma in a Chinese population. *Int J Ophthalmol* 2026;19(7):1344-1350

INTRODUCTION

Optic disc melanocytoma (ODM) is a benign, deeply pigmented intraocular tumor composed of nevus-like melanocytic cells[1-4]. The lesion is typically located on the optic disc and may extend into the adjacent optic nerve head. Its clinical features are well recognized; however, advances in multimodal fundus imaging have provided further insights into its structural and functional characteristics.

In this study, multimodal imaging findings in 69 eyes with ODM were analyzed. To our knowledge, this represents the largest case series reported in China to date. The purpose of this study was to characterize the clinical and imaging features of ODM in a Chinese population and to further refine the classification of tumor-retina interface patterns based on optical coherence tomography (OCT) findings.

PARTICIPANTS AND METHODS

Ethical Approval This study adhered to the tenets of the Declaration of Helsinki and was approved by the Ethics Committee of Beijing Tongren Hospital, Capital Medical University [Ethics approval No.TRECKY2018-056-GZ (2022)-07]. Written informed consent was obtained from all participants.

Participants Totally 69 consecutive patients (69 eyes) diagnosed with ODM between January 2015 and December 2025 were retrospectively reviewed. Diagnosis was established based on clinical examination and multimodal imaging findings[1,3-6]. Inclusion criteria were defined as follows: visual

complaints directly attributable to the tumor itself were rare; however, visual symptoms were permitted if they could be explained by tumor-related secondary fundus complications. On ophthalmoscopic examination, lesions were characterized as mildly elevated, gray-to-black pigmented masses originating from the optic disc and confined to the disc or extending into the adjacent peripapillary retina. No associated exudative retinal detachment was observed. On B-scan ultrasonography, tumor thickness was typically less than 2 mm, and acoustic hollowness was generally absent.

Imaging Protocol All patients underwent comprehensive ophthalmic examination, including best-corrected visual acuity, intraocular pressure measurement, slit-lamp biomicroscopy, indirect ophthalmoscopy, 45° color fundus photographs centered on macular and optic disc (Type CR6-45NM, Canon Inc., USA), and spectral-domain OCT (Spectralis; Heidelberg Engineering, Heidelberg, Germany). Additional imaging modalities, including fundus autofluorescence, near-infrared reflectance imaging, fundus fluorescein angiography (FFA), indocyanine green angiography (ICGA), B-scan ultrasonography, and visual field testing, were performed as clinically indicated.

Clinical Evaluation and Measurements Tumor characteristics evaluated included color, size, extent of disc involvement, and associated ocular complications. On 45° color fundus photographs centered on the optic disc, quantitative analysis was performed using ImageJ software (National Institutes of Health, Bethesda, MD, USA). The margins of the optic disc and the tumor were manually delineated on the original-resolution images, and the maximal diameter (in pixels) as well as the area (in pixels) were measured for each. Using the optic disc as an internal reference standard, tumor size was expressed relative to disc size: the maximal tumor diameter was calculated in disc diameters, and the tumor area was calculated in disc areas. In cases where the optic disc of the affected eye was partially or completely obscured by the tumor and could not be reliably delineated, a color fundus photograph of the contralateral eye obtained under the same imaging settings and magnification was used as a reference. The optic disc margin of the fellow eye was outlined and proportionally transposed to the corresponding anatomical location in the affected eye image. Measurements were then performed accordingly to ensure methodological consistency and reproducibility.

Radial OCT scans centered on the fovea and the optic disc were obtained for all eyes. Each radial scan protocol consisted of 6 to 12 B-scans evenly distributed over 360 degrees, with a scan length of approximately 6–9 mm, depending on the size of the lesion. Each B-scan comprised approximately 512 A-scans. Automatic real-time averaging (typically 9–15 frames) was applied to enhance image quality and reduce noise. All scan orientations were reviewed. Only images with sufficient signal strength and clear visualization of the tumor–retina interface were included in the analysis.

On radial B-scan images centered on the optic disc, the extent of tumor involvement within the retinal layers was analyzed, and the morphological characteristics of the tumor–retina interface were carefully assessed. Due to shadowing artifacts caused by the highly pigmented lesion, involvement of the choroid could not be reliably evaluated.

Retinal edema, retinoschisis, and the presence of epiretinal membrane (ERM) were systematically evaluated using color fundus photography and OCT. Vitreous seeding was defined as the presence of disseminated pigmented granules outside the tumor margin on color fundus photography, or as scattered hyperreflective particles within the vitreous cavity detected on OCT imaging.

B-scan ultrasonography was performed using the MyLab 90 system (Esaote, Italy). Transverse and longitudinal scans were obtained through the lesion in multiple orientations to ensure comprehensive evaluation. Tumor dimensions, including basal diameter and thickness, were assessed. Internal reflectivity, homogeneity, the presence of acoustic hollowness, choroidal excavation, and posterior acoustic features were qualitatively evaluated.

Statistical Analysis Statistical analysis was performed using SPSS version 27.0 (IBM Corp., Armonk, NY, USA). Continuous variables are presented as mean±standard deviation, and categorical variables as frequencies and percentages.

RESULTS

General Clinical Characteristics A total of 69 patients (69 eyes) with ODM were included in this study. There were 49 females (71.0%) and 20 males (29.0%), with a mean age of 47.8±12.1y (range, 17–70y). Fifty-four patients (78.3%) were referred after detection of an optic disc mass during routine ophthalmic examination, 4 patients (5.8%) presented with complaints of floaters, and 11 patients (15.9%) presented with decreased visual acuity. None of the patients had associated systemic diseases.

Ocular Findings All patients had unilateral involvement, including 34 right eyes (49.3%) and 35 left eyes (50.7%). The mean visual acuity of the affected eyes was 0.8±0.3. Among them, 55 eyes (79.7%) had visual acuity ≥0.8, 8 eyes (11.6%) had visual acuity between 0.2 and 0.7, and 6 eyes (8.7%) had visual acuity ≤0.1.

Multimodal Fundus Imaging Findings All lesions appeared black or gray in color. Thirty-nine cases (56.5%) demonstrated uniformly black pigmentation, whereas the remaining 30 cases (43.5%) exhibited heterogeneous gray-black pigmentation,

reflecting variable depths of retinal involvement within different regions of the tumor (Figure 1).

Color fundus photography showed that only one patient (1.4%) had a lesion confined entirely within the optic disc. The remaining 68 patients (98.6%) had lesions extending beyond the disc margin, involving an average of 7.1±3.1 clock hours of the disc circumference. Feathery tumor margins were observed in 19 patients (27.5%).

The mean maximum tumor diameter was 1.7±0.6 disc diameters (range, 0.38–3.49 disc diameters), and the mean tumor area was 3.0±2.2 disc areas (range, 0.16–11.69 disc areas).

Three patients (4.3%) had concurrent choroidal nevi. Secondary fundus findings included optic disc edema in 48 patients (69.6%), thinning of the retinal nerve fiber layer (RNFL) corresponding to the tumor location in 39 patients (56.5%), retinal vascular sheathing within the tumor in 23 patients (33.3%), retinal exudation in 4 patients (5.8%), ERM in 5 patients (7.2%), and vitreous seeding of tumor cells in 9 patients (13.0%; Figure 2).

Fifty-eight patients (84.1%) underwent OCT examination. OCT images demonstrated a prominently elevated mass at the optic disc, covered by a variably thick and structurally disorganized retinal layer. The tumor–retina interface appeared as a hyperreflective band, with dense posterior shadowing beneath the lesion.

Based on the extent of retinal involvement and the qualitative morphological characteristics of tumor cell distribution at the anterior tumor margin, three OCT patterns of the tumor–retina interface were identified. When the tumor involved the RNFL, the anterior tumor surface appeared as a smooth hyperreflective band, with no overlying retinal tissue detectable on OCT. In such cases, the tumor typically appeared deeply pigmented on color fundus photography and was often associated with a feathery margin. When the tumor did not involve the RNFL, two patterns were observed depending on the arrangement of tumor cells. In cases where the tumor cells appeared relatively compact and densely organized, the interface presented as a nodular hyperreflective band. In contrast, when the tumor cells were more loosely arranged, the interface demonstrated a honeycomb-like pattern of hyperreflective foci (Figure 1). On color fundus photography, both patterns generally appeared gray, with the honeycomb-like pattern tending to show a lighter gray appearance. It should be noted that the distinction between nodular and honeycomb-like patterns represents a continuum of morphological appearances rather than strictly defined categories.

Different regions within the same tumor could exhibit different OCT patterns. Among the 69 cases, 27 (39.1%) showed a smooth hyperreflective interface, 34 (49.3%) showed a nodular hyperreflective interface, and 9 (13.0%) showed a honeycomb-like hyperreflective pattern.

Peripapillary hyperreflective ovoid mass-like structures (PHOMS) were observed in 11 patients (15.9%), all located adjacent to edematous optic disc tissue (Figure 2).

Fifteen patients underwent B-scan ultrasonography. The mean maximum basal diameter was 3.84±0.79 mm (range, 2.5–5.6 mm), and the mean tumor height was 1.68±0.37 mm (range, 0.9–2.3 mm). All tumors appeared as solid lesions with homogeneous medium-to-high internal reflectivity. No cases demonstrated acoustic hollowness or choroidal excavation. Blood flow signals within the tumor were detected in 13 patients (86.7%).

Twenty-nine patients underwent near-infrared reflectance imaging. Sixteen patients (55.2%) demonstrated fibrous hyperreflectivity aligned with the course of the RNFL, 7 patients (24.1%) showed mottled hyperreflectivity, and 6 patients (20.7%) showed band-like hyperreflectivity.

Ten patients underwent fundus autofluorescence, FFA, and ICGA examinations. All cases showed uniformly hypoautofluorescent lesions on fundus autofluorescence imaging. On FFA, 9 cases demonstrated early hypofluorescence with telangiectatic leakage over the optic disc surface, and partial late staining of the tumor. One case remained hypofluorescent throughout the entire angiographic study. On ICGA, all cases showed persistent hypofluorescence throughout all phases (Figure 3). No definite intrinsic tumor vasculature was identified on either FFA or ICGA.

Six patients underwent visual field testing. One patient had a normal visual field, one had a scotoma contiguous with the physiologic blind spot, two had nerve fiber bundle defects, and two had quadrant visual field defects. All visual field defects corresponded to the tumor location and areas of RNFL thinning (Figure 3).

DISCUSSION

This study presents the largest case series of ODM in a Chinese population to date and provides a comprehensive characterization of its multimodal imaging features. The demographic profile and overall clinical characteristics in our cohort were largely consistent with those reported in other ethnic populations[1,4,7]. However, tumors in our series appeared slightly larger, and two relatively uncommon complications, PHOMS and ERM, were observed with notable frequency.

ODM is typically detected incidentally during routine ophthalmic examination, although a subset of patients presents with visual symptoms[1]. In our cohort, 15.9% of patients reported decreased visual acuity, primarily attributable to secondary retinal complications rather than direct tumor infiltration. Despite a high prevalence of RNFL thinning (56.5%), subjective visual field complaints were relatively

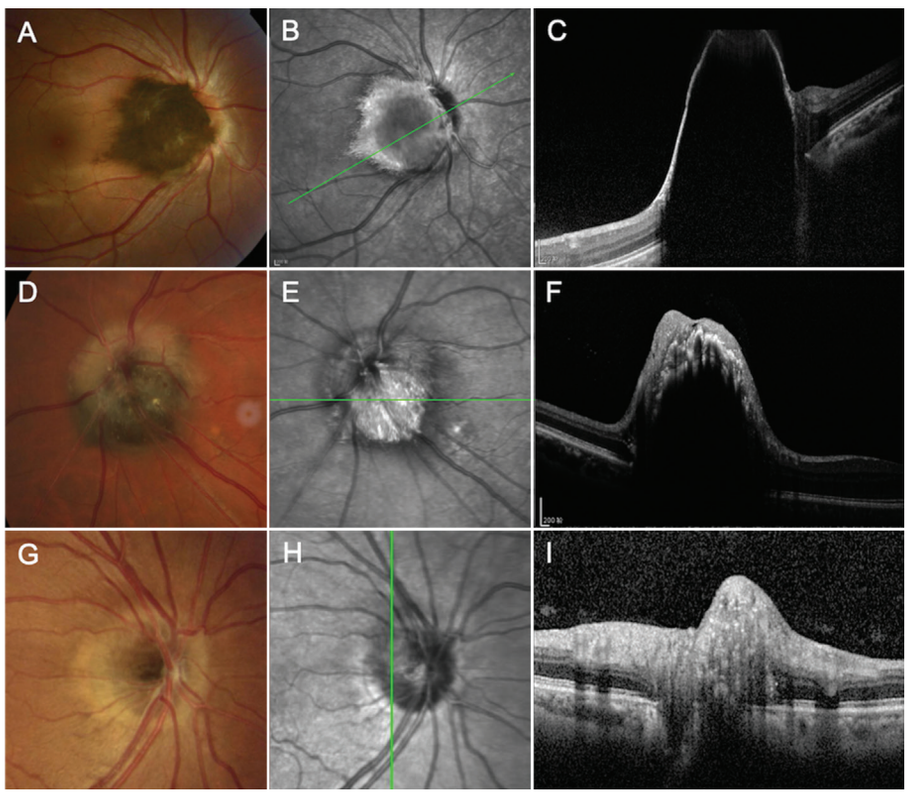

Figure 1 CFP, IRF, and OCT images of optic disc melanocytoma A: CFP showing a uniformly black optic disc melanocytoma with feathery margins; B: IRF image corresponding to A, demonstrating fibrillar hyperreflectivity; the green arrow indicates the direction of the OCT scan; C: OCT B-scan corresponding to the green arrow in B, showing a thin and smooth hyperreflective anterior tumor surface; D: CFP revealing a dark gray tumor associated with optic disc edema; E: IRF image demonstrating band-like hyperreflectivity within the lesion; F: OCT image showing that the tumor does not involve the retinal nerve fiber layer; the anterior surface exhibits nodular hyperreflectivity; G: CFP demonstrating a lighter-colored tumor confined within the optic disc; H: IRF image showing focal patchy hyperreflectivity; I: OCT image revealing honeycomb-like hyperreflective dots within the lesion. CFP: Color fundus photography; IRF: Infrared reflectance; OCT: Optical coherence tomography.

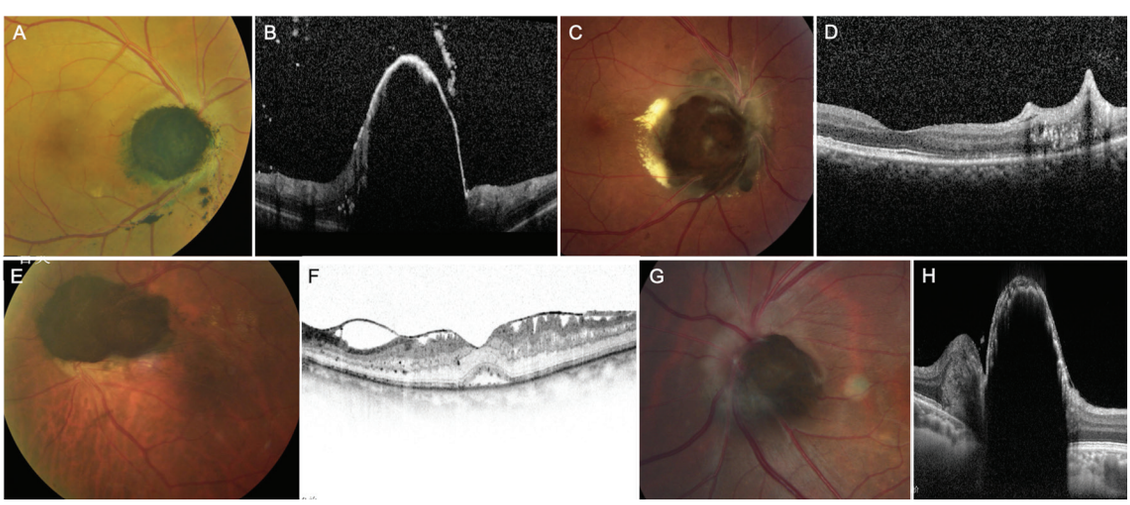

Figure 2 Color fundus photography and optical coherence tomography images of fundus complications secondary to optic disc melanocytoma A, B: Vitreous seeding; C, D: Hard exudates; E, F: Epiretinal membrane; G, H: Peripapillary hyperreflective ovoid mass-like structures.

uncommon, suggesting that slow tumor growth allows for partial functional adaptation. Visual field defects, when present, corresponded topographically to areas of RNFL compression, supporting a mechanical rather than infiltrative mechanism of optic nerve dysfunction[2,5].

A notable finding of our study was the larger tumor basal diameter compared with previously reported series. The mean basal diameter and thickness in our cohort exceeded those reported in predominantly White and Black populations. The mean basal diameter and thickness in our study were 3.84 mm

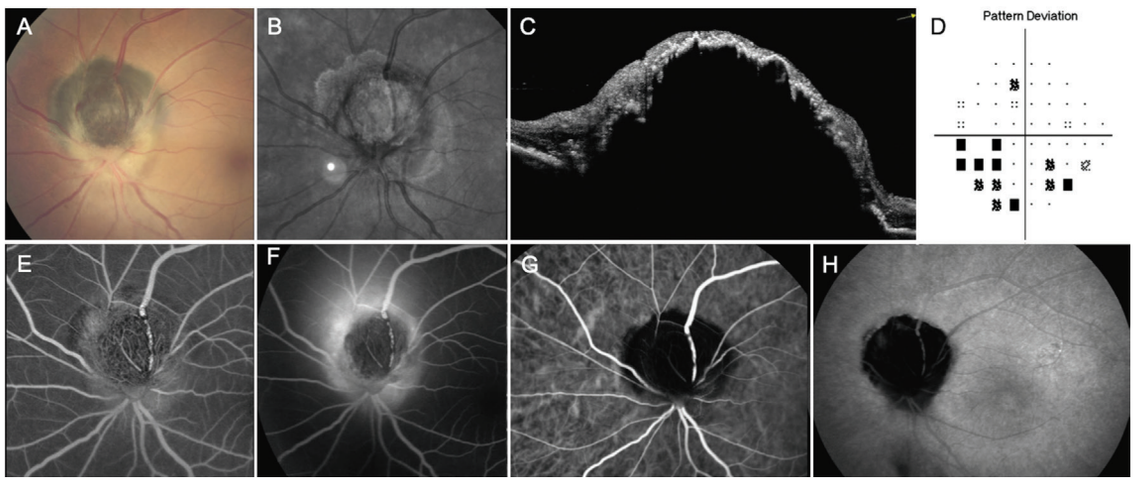

Figure 3 Multimodal imaging features of optic disc melanocytoma A: Color fundus photograph showing a black elevated lesion involving the superior half of the optic disc, associated with a superior retinal nerve fiber layer defect and inferior optic disc edema; B: Infrared reflectance image demonstrating fibrillar hyperreflectivity; C: Optical coherence tomography image revealing nodular hyperreflectivity on the tumor surface with marked posterior shadowing; D: Visual field examination showing an inferior arcuate visual field defect; E: Early-phase fundus fluorescein angiography demonstrating hypofluorescence of the tumor with dilated superficial disc capillaries; F: Late-phase fundus fluorescein angiography showing persistent tumor hypofluorescence with leakage from the superficial disc capillaries; G, H: Indocyanine green angiography images from early to late phases demonstrating persistent hypofluorescence of the tumor.

and 1.68 mm, respectively. Shields *et al*[1,3], in predominantly White and Black populations, reported a mean basal diameter of 2.0–2.6 mm and thickness of approximately 1.0–1.9 mm. Lee *et al*[4] reported a median diameter of 3.1 mm (range 1.6–4.4 mm) and median height of 1.9 mm (range 0.8–2.4 mm) in Korean patients. Several factors may account for this discrepancy. First, differences in healthcare access and screening practices may result in later detection. Second, referral bias at our tertiary center may have enriched the sample with larger or diagnostically uncertain lesions. The relatively larger tumor size in our cohort may account for the markedly lower proportion of lesions confined entirely within the optic disc (1.4%) compared with that reported in previous studies (13.4%–40.0%)[6].

Although the mean basal diameter of ODM in our study was slightly larger than that reported in some previous studies, the tumor height was comparable to prior reports. Previous literature on ODM consistently demonstrates that the elevation at initial presentation is typically less than 2 mm, underscoring its benign nature. This represents one of the key distinguishing features from choroidal melanoma.

These findings further highlight the importance of B-scan ultrasonography in the diagnosis of ODM. Due to the shadowing effect caused by dense melanocytic pigmentation, OCT is unable to reliably delineate the posterior tumor margin. Moreover, given the typically small size of ODM, the spatial resolution of magnetic resonance imaging is insufficient for accurate measurement of tumor dimensions. In addition, ultrasonography characteristically demonstrates solid lesions with medium-to-high internal reflectivity within ODM, along with the absence of acoustic hollowness and choroidal excavation, all of which are helpful features in differentiating ODM from choroidal melanoma.

A key contribution of this study is the systematic classification of tumor–retina interface patterns on OCT. While previous studies described a nodular hyperreflective anterior surface as a characteristic OCT feature[3], we identified three reproducible patterns: smooth hyperreflective, nodular hyperreflective, and honeycomb-like hyperreflective. We propose that these patterns reflect variations in the depth of retinal involvement and the density of tumor cell distribution at the anterior tumor surface.

When the tumor infiltrates the RNFL and tumor cells are densely compacted, the anterior interface appears as a thin, smooth hyperreflective band. In contrast, when the RNFL is spared but anterior tumor cells remain densely arranged, the interface appears nodular. When the tumor did not involve the RNFL and anterior tumor cells were loosely arranged, the interface demonstrated a honeycomb-like pattern of hyperreflective foci.

Shields *et al*[3] previously reported using time-domain OCT that thicker tumors displayed thinner anterior hyperreflective borders and denser shadowing. We believe this corresponds to the thin, smooth hyperreflective band observed in our study, reflecting dense distribution of pigment-rich tumor cells within the RNFL. This pattern accounted for 39.1% of cases. The classic nodular hyperreflective interface[8-9] was the most common pattern, accounting for 49.3% of cases.

Histopathologic studies have demonstrated that when the tumor surface appears irregular on OCT, it corresponds to less densely packed tumor architecture with reduced cellular cohesion. This pattern correlates with nodular hyperreflectivity, whereas even poorer cellular cohesion corresponds to the honeycomb-like pattern. Okubo *et al*[10] described multiple hyperreflective dots of varying sizes within the elevated retina overlying the tumor in five cases of ODM, particularly in lesions with lighter pigmentation and tumor margins located within the outer retina. These hyperreflective dots corresponded histopathologically to gliotic degeneration and increased pigmentation, and were considered to represent melanophages and/or tumor cells. This finding is similar to the honeycomb-like hyperreflectivity described in our study.

Although OCT provides limited visualization of the internal tumor architecture due to dense pigmentation and posterior shadowing, it remains highly valuable for detecting associated retinal complications. The relatively high prevalence of PHOMS (15.9%) in our cohort warrants particular attention. This represents a recently recognized peripapillary finding in ODM[11-12]. Zhang *et al*[11] reported that PHOMS was detected in 88.2% of 30 ODM patients using swept-source OCT, which was significantly higher than in fellow eyes (17.1%).

PHOMS have been proposed to be associated with impaired axoplasmic flow and possible mechanical effects on optic nerve fibers[13-14]. Given that ODM frequently involves the optic nerve head and adjacent regions, it is plausible that local structural alterations may contribute to the development of PHOMS. However, in the absence of OCT angiography (OCTA) data in the present study, potential perfusion- or flow-related mechanisms cannot be evaluated. Therefore, these interpretations should be considered speculative and hypothesis-generating. The relatively larger tumor size in our series may have contributed to the higher rate of optic disc edema compared with prior reports[1,6], which may also be associated with the occurrence of PHOMS.

Five patients (7.2%) developed ERM in the affected eyes, whereas no ERM was observed in fellow eyes. Lee *et al*[4] reported ERM in 2 of 27 Korean patients (7%). Prasannan *et al*[15] reported a case of ODM associated with ERM and full-thickness macular hole, in which pars plana vitrectomy with internal limiting membrane peeling revealed a tightly adherent internal limiting membrane; histopathology showed predominantly spindle-shaped cells with delicate eosinophilic fibrillary cytoplasm. More recently, Zhang *et al*[11] reported an ERM incidence of 20.6% in 34 ODM patients. The mechanism underlying ERM formation in ODM remains unclear. We speculate that ODM alters the peripapillary microenvironment, stimulating glial proliferation on the retinal surface, which may lead to ERM formation and possibly macular hole development.

Furthermore, in the present study, 4.3% of patients had concurrent choroidal nevi. In our clinical observations, ODM may coexist with choroidal nevi, which may be explained by the fact that both entities represent melanocytic nevi differing primarily in their anatomical location. Although there are limited reports specifically addressing the coexistence of ODM and choroidal nevus, Shields *et al*[1] reported that ocular melanocytosis was present in 8% of patients in a series of 115 cases of ODM. Notably, ODM, choroidal nevus, and ocular melanocytosis all represent benign proliferations of melanocytes, which may partly explain their occasional concurrence.

ODM typically demonstrates uniformly hypoautofluorescent signals on fundus autofluorescence, primarily attributable to the masking effect of dense melanocytic pigmentation. This feature may assist in differentiating ODM from choroidal melanoma. In contrast, choroidal melanoma frequently shows slight intrinsic hyperautofluorescence, which is associated with retinal pigment epithelium dysfunction and the accumulation of lipofuscin over the tumor surface[16].

The angiographic findings in our series were consistent with established literature[1]. Persistent hypofluorescence on FFA and ICGA reflects the densely pigmented, poorly vascularized nature of ODM.

Our unpublished data indicate that ODM accounts for approximately 2.4% of all intraocular melanocytic tumors, ranking second only to uveal melanoma. Therefore, accurate recognition of its clinical features is of clinical importance, particularly in distinguishing it from uveal melanoma. Multimodal imaging plays a central role in the evaluation and differential diagnosis of ODM. Color fundus photography remains the essential first-line modality, as it documents lesion size, pigmentation, margins, and fundus complications. OCT further delineates retinal involvement and tumor-retina interface characteristics, while B-scan ultrasonography provides reliable thickness measurement, with ODM generally measuring less than 2 mm and lacking acoustic hollowness or choroidal excavation. Fundus autofluorescence and other ancillary tests may be selectively used in challenging cases. These imaging features collectively support the diagnosis of ODM and assist in differentiating it from melanoma.

This study has several limitations. First, its retrospective design introduces potential selection bias, and imaging protocols were not entirely uniform across all cases. Second, not all patients underwent comprehensive multimodal imaging, which may have led to an underestimation of certain complications. In particular, OCTA was not performed; however, OCTA plays a role in the differential diagnosis of retinal and choroidal diseases[17-19], and its absence limited the

assessment of microvascular and perfusion-related changes, thereby constraining the mechanistic interpretation of findings such as PHOMS. Third, histopathologic confirmation was not available, and imaging-based interpretation of structural patterns remains inferential. Future prospective studies incorporating standardized imaging protocols, longitudinal follow-up, and advanced modalities such as swept-source OCTA are warranted to further elucidate the natural history, vascular characteristics, and structural evolution of ODM.

In conclusion, ODM in Chinese patients demonstrates clinical and imaging characteristics comparable to those described in other populations, with the notable distinction of slightly larger tumor dimensions. The identification of three distinct OCT tumor–retina interface patterns and the recognition of PHOMS and ERM as associated findings expand current understanding of ODM pathophysiology and may have implications for imaging-based monitoring and risk assessment.

ACKNOWLEDGEMENTS

Foundations: Supported by the National Natural Science Foundation of China (No.82220108017; No.82141128); the Capital Health Research and Development of Special (No.2024-1-2052); Science & Technology Project of Beijing Municipal Science & Technology Commission (No.Z201100005520045); Sanming Project of Medicine in Shenzhen (No.SZSM202311018).

Conflicts of Interest: Yan YN, None; **Liu YM,** None; **Wei WB,** None.

REFERENCES

1 Shields JA, Demirci H, Mashayekhi A, *et al*. Melanocytoma of optic disc in 115 cases: the 2004 Samuel Johnson Memorial Lecture, part 1. *Ophthalmology* 2004;111(9):1739-1746.

2 Osher RH, Shields JA, Layman PR. Pupillary and visual field evaluation in patients with melanocytoma of the optic disc. *Arch Ophthalmol* 1979;97(6):1096-1099.

3 Shields CL, Perez B, Benavides R, *et al*. Optical coherence tomography of optic disk melanocytoma in 15 cases. *Retina* 2008;28(3):441-446.

4 Lee CS, Bae JH, Jeon IH, *et al*. Melanocytoma of the optic disk in the Korean population. *Retina* 2010;30(10):1714-1720.

5 Kwak JJ, Lee DH, Lee SC, *et al*. Evaluation of blood vessel network formation and visual field defect in optic disc melanocytoma. *Br J Ophthalmol* 2023;107(3):418-424.

6 Finger PT, Natesh S, Milman T. Optical coherence tomography: pathology correlation of optic disc melanocytoma. *Ophthalmology* 2010;117(1):114-119.

7 Mazzini C, Vicini G, Nicolosi C, *et al*. Multimodal imaging of optic disc melanocytoma. *Eur J Ophthalmol* 2021:11206721211010616. Epub ahead of print.

8 Filloy A, Arias L, Ascaso FJ, *et al*. Swept source optical coherence tomography imaging of optic disc melanocytoma. *Clin Exp Ophthalmol* 2017;45(3):313-314.

9 Apinyawasisuk S, McCannel T, Arnold AC. Clinical and spectral-domain optical coherence tomography appearance of optic disc melanocytoma: a new classification and differentiation from pigmented choroidal lesions. *Ocul Oncol Pathol* 2017;3(2):142-148.

10 Okubo A, Unoki K, Yoshikawa H, *et al*. Hyperreflective dots surrounding the central retinal artery and vein in optic disc melanocytoma revealed by spectral domain optical coherence tomography. *Jpn J Ophthalmol* 2013;57(1):108-112.

11 Zhang R, Dong J, Li Y, *et al*. Optical coherence tomography and optical coherence tomography angiography features of optic disc melanocytoma: peripapillary hyperreflective ovoid mass-like structures, perfusion deficits, and association with vision loss. *Am J Ophthalmol* 2025;280:238-247.

12 Wang F. Case report: optic disc melanocytoma with PHOMS—minimum intensity projection image. *Int Med Case Rep J* 2024;17:137-141.

13 Jonas JB, Panda-Jonas S, Milea D, *et al*. Peripapillary hyperreflective ovoid mass-like structures: prevalence and associations in the adult population of the Beijing eye study. *Invest Ophthalmol Vis Sci* 2025;66(6):63.

14 Gernert JA, Christmann T, Kaufmann E, *et al*. Characterization of peripapillary hyperreflective ovoid mass-like structures in a broad spectrum of neurologic disorders. *Ophthalmology* 2025;132(5):590-597.

15 Prasannan V, Brar AS, Padhy SK. Optic disc melanocytoma associated with full thickness macular hole. *Clin Exp Optom* 2024;107(8):866-867.

16 Shields CL, Bianciotto C, Pirondini C, *et al*. Autofluorescence of choroidal melanoma in 51 cases. *Br J Ophthalmol* 2008;92(5):617-622.

17 Gündüz AK, Mirzayev I, Kasimoglu R, *et al*. Swept-source optical coherence tomography angiography findings in choroidal and retinal tumors. *Eye (Lond)* 2021;35(1):4-16.

18 Tsai TY, Tsai YJ, Chu YC, *et al*. Ocular circulation change in optic disc melanocytoma–a case report and a review of the literature. *BMC Ophthalmol* 2023;23(1):33.

19 Cennamo G, Montorio D, D'Andrea L, *et al*. The role of OCT angiography in a rare case of malignant trasformation of an optic disc melanocytoma. *Photodiagnosis Photodyn Ther* 2021;33:102089.